

Tailoring the Viscoelasticity of Epoxy Thermosets

J. S. Nakka,¹ K. M. B. Jansen,² L. J. Ernst¹

¹Mechanical Engineering Dept., Delft University of Technology, Mekelweg 2, 2628 CD Delft, The Netherlands

²Industrial Design Engineering, Delft University of Technology, Landbergstraat 15, 2628 CE Delft, The Netherlands

Correspondence to: J. S. Nakka (E-mail: j.s.nakka@tudelft.nl)

ABSTRACT: This research work is aimed to understand the effect of epoxy resin chemistry on the viscoelasticity of the cured epoxy thermosets. In this article, two model systems are selected based on epoxy-amine reactants. In the model Systems I, the functionality of the epoxy is varied. In model System II, the pendant (side) chain length in the amine is varied. It is found that by varying the initial properties (e.g., functionality, pendant chain length, mixing ratio (r), aromaticity, etc.) the network properties (crosslink density and flexibility) of the cured (or hardened) epoxy changed. The changes (or shift) in the viscoelastic properties (or viscoelasticity) of the cured epoxy is mainly due the changes in the network properties. Further, to study the time and temperature effects the viscoelastic master curves for the two model systems are generated using Time-Temperature-Superposition (TTS) principle. The shift in the viscoelastic master curves is modeled with a simple Kohlrausch-Williams-Watts (KWW) fit function. © 2012 Wiley Periodicals, Inc. *J. Appl. Polym. Sci.* 128: 3794–3806, 2013

KEYWORDS: thermosets; crosslinking; structure–property relations; glass transition; viscosity and viscoelasticity

Received 18 July 2012; accepted 6 August 2012; published online 12 October 2012

DOI: 10.1002/app.38435

INTRODUCTION

Epoxy resins are used for many important applications such as encapsulation of electronic devices, structural aerospace materials and in coatings industries.^{1–6} The epoxy resin contains reactive monomers which can undergo chemical reaction upon heating. Epoxy thermosets are formed by heating (or curing) the epoxy resins. Also, the epoxy thermosets can be made by mixing the epoxy resin with the hardener (or curing agent). The examples of hardeners are amine, phenolic, imines, anhydrides, etc. Epoxy thermosets are polymeric materials whose properties (mechanical, thermal, etc.) depend on time and temperature. Epoxy thermosets show both elastic and viscous (i.e., visco-elastic) properties with respect to time and temperature. The visco-elastic response is commonly known as viscoelasticity. Viscoelasticity plays a vital role in the long-term performance of the epoxy thermosets. The position of the viscoelastic transition region is characteristic for the determining the thermo-mechanical properties of these thermoset materials. The viscoelasticity of epoxy thermosets depends mainly on the network structure which is formed after the cure reaction between the epoxy resin and curing agent. The network structure formed depends on the initial properties of the reacting epoxy resin-curing agent mixture. The viscoelastic response of epoxy resins cured with various curing agents has been studied in the past by many researchers.^{7–9}

From our previous studies and also from other research work it was found that the viscoelastic response of the cured epoxies is

sensitive to the variation of the reacting mixture (or group) functionalities, mixing ratios, conversion, curing conditions, and the crosslink density of the network formed.^{10–15}

In our previous work,^{10,11} model systems are selected based on epoxy-amine reactants. In the first model system¹⁰ the average functionality of the epoxy (Bisphenol A diglycidyl ether; BADGE) resin is $f_E = 2$. While the functionality of the amine reactant (or hardener) is varied from $f_A = 2$ to $f_A = 4$. The viscoelasticity of the epoxy-cured samples are determined using the dynamic mechanical analyzer (DMA). It was found that with the increase in the functionality of the amine the viscoelasticity of the cured epoxy changed. The glassy modulus remained constant. The glass transition temperature (T_g) increased by 42°C. And the rubbery modulus (E_r) increased from 11 to 35 MPa. The increase in the T_g and E_r is due to the change in the network property i.e., crosslink density (ν_C). The ν_C increased from $\sim 1000 \text{ mol/m}^3$ to $\sim 3200 \text{ mol/m}^3$.

In the second model system,¹¹ the functionality of the epoxy resin and the amine hardener is kept constant i.e., $f_E = 2$ and $f_A = 4$. While, the chain length of the amine hardener is varied via the selection of homologous series of amines. The viscoelasticity of the cured epoxy has changed by varying the chain length of the amine hardener. It is found that the E_g and E_r remained constant. The T_g decreased by 28°C with the increase in the chain length of the amine hardener. A slight decrease from 2800 mol/m^3 to 3200 mol/m^3 in the ν_C is observed. It is found that

the change in the viscoelasticity is mainly due to introduction of the flexibility (F) in the epoxy network. Both the ν_C and F parameters are used to predict the T_g of the cured epoxies.

In this article, two model systems are selected based on epoxy-amine reactants (see Table I). In the model System I, the average functionality of the epoxy is varied from $f_E = 2$ to $f_E = 4$ and the functionality of amine is kept constant $f_A = 2$. In model System II, the functionality of the epoxy and amine is kept constant i.e., $f_E = 2$ and $f_A = 3$. While, the pendant (side group) aliphatic chain length of the amine reactant is varied. The summary of the two model systems selected based on initial properties i.e., functionality, mixing ratio, and aromaticity etc., are shown in the Table II. The changes in the viscoelasticity of the cured epoxy samples from the two model systems are analyzed with respect to the network properties i.e., ν_C and F . Furthermore, the viscoelasticity of the two model systems are predicted.

The epoxy materials that are used for high tech applications such as in aerospace and electronic industry must satisfy stringent specifications regarding dimensions, warpage, and high temperature behavior. Hence any change in the initial epoxy composition immediately varies and affects the final viscoelasticity. Such batch to batch variations in the epoxy composition can easily occur in the suppliers' production process. The aim is to understand the effect of the initial epoxy resin chemistry on the viscoelasticity of their cured products. This understanding gives a first hand estimate of the final properties and thereby saves time for the characterization of the polymeric materials which is tedious. Moreover, if a good understanding of the relation between the epoxy resin chemistry and the final properties of the cured product is known then it would be possible to be able to predict the properties. Furthermore, it is also possible to tailor the properties of the polymeric materials. Although this research work cannot be generalized to all kinds of polymeric materials, it gives the knowledge to understand and predict the properties within a class of epoxy polymeric materials which can help us in the selection of the right material for the desired end application.

EXPERIMENTAL

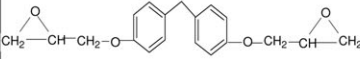
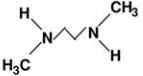
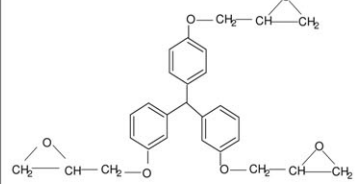
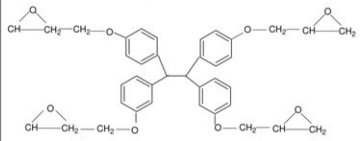
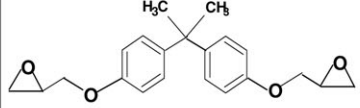
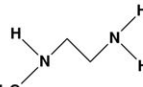
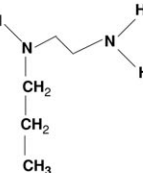
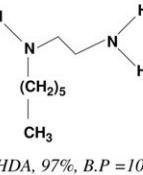
Materials

The epoxy resins that are selected for the present study are Bisphenol A diglycidyl ether (BADGE, 97%), Bisphenol F diglycidyl ether (BFDGE, 98%), Tris (4-hydroxyphenyl) methane triglycidyl ether (TMTE, 98%), and Tetra phenylmethane glycidyl ether (TPGE, 95%) are shown in Table I. The amines that are selected are *N,N'*-Dimethylethylene diamine (DMEDA, 99%), *N*-Methylethylene diamine (MEDA, 95%), 1, 2-Diamino Ethane (EDA, 99%), *N*-Propylethylene diamine (NPDA, 97%), and *N*-Hexylethylene diamine (NHDA, 97%) as shown in Table I. The epoxy resins and amines are purchased from Sigma-Aldrich Logistik GmbH, Schnellendorf, Germany. The curing reaction between epoxy and amine is shown in Figure 1.

Sample Preparation

Neat resin castings for DMA studies were prepared in aluminum moulds. The aluminum mould consist of an aluminum

Table I. Selection of Resin and Curing Agents for Model Systems

Model System	Chemical Structure of Resin, Name, Purity, M.P ($^{\circ}$ C), functionality, M_w (g/mol), ρ (g/cm 3)	Chemical Structure of hardener Name, Purity, B.P ($^{\circ}$ C), functionality, M_w (g/mol), ρ (g/cm 3)
I	 BFDGE, 98% ^t , M.P=46, $f_E=2$, $M_w=312.37$, $\rho=1.19$	 DMEDA, 99%, B.P=119, $f_A=2$, $M_w=88.15$, $\rho=0.819$
	 TMTE, 98% ^t , M.P= 49, $f_E=3$, $M_w=460.53$, $\rho=1.25^t$	
	 TPGE, 95% ^t , M.P= 80, $f_E=4$, $M_w=622.7$, -	
II	 BADGE, 99%, M.P=40, $f_E=2$, $M_w=340.41$, $\rho=1.16$	 MEDA, 95%, B.P=115, $f_A=3$, $M_w=74.13$, $\rho=0.850$
		 NPDA, 97%, B.P=148, $f_A=3$, $M_w=102$, $\rho=0.829$
		 NHDA, 97%, B.P=102, $f_A=3$, $M_w=144.26$, $\rho=0.832$

Note: M_w , ρ , M.P, B.P and ^t are molecular weight, density, melting, and boiling points and tentative values.

Table II. Model System Numbers, Constant, and Variable Parameters, Code, Post Cure Schedule, Epoxy/Amine Functionality, Density

Model system	Constant parameters	Variable parameters	Code	Post cure schedule	epoxy/amine functionality	Density(ρ) (g/cm ³)
I	Acyclic nature	Aromaticity, r , f_E , CS	E2	100_4H	2/2	1.207
			E2.5	120_2H	2.5/2	1.212
			E3	150_2H	3/2	1.217
			E4	200_8H	4/2	-
II	f_E , f_A , Aromatic and Acyclic nature	Substituent Chain length	P1	150_4H	2/3	1.191
			P3	200_2H	2/3	1.175
			P6	200_4H	2/3	1.152

f_E , f_A , r , and CS are functionality of epoxy, amine, mixing ratio, and cure schedule.

insert with gaps of dimension $6.0 \times 1.5 \times 3 \text{ mm}^3$ and is fastened in between two aluminum plates into which the premixed resin is poured and cured at different curing schedules. High temperature mirror glaze wax, (Meguiar's, Irvine, USA) is used as mould releasing agent. First, a known amount of epoxy resin is taken in a beaker. Some of selected epoxies crystallize at room temperature. Therefore, all the selected epoxy resins are heated at 80°C for half an hour so that the epoxy crystals melt and also the absorbed moisture is removed. To this a stoichiometric amount of amines is added and mixed thoroughly. The prepared mixture is then cast in the aluminum mould. Then they are cured and post cured at different temperatures in order to obtain full conversion of the epoxy. Initially, cured samples of stoichiometrically mixed amines and epoxy are prepared with

different mixing ratios and cure schedules. For all formulations containing different mixing ratios curing is done initially at 80°C for 3 h and 100°C for 1 h and then post cured. Table II shows the different mixing ratios and post curing temperatures. Preliminary measurements showed that too high post cure temperature ($>150^\circ\text{C}$) for the lower functionality resins resulted in the undesired etherification reaction shown in Figure 1(c). The samples which have undergone etherification reactions showed two $\tan \delta$ peaks during the DMA characterization. The two $\tan \delta$ peaks indicate inhomogeneous network. The inhomogeneous network is formed due to the etherification reaction and epoxy-amine reaction. To avoid etherification, the post cure temperature is done according to Table II such that a single $\tan \delta$ peak due to epoxy-amine reaction is achieved during the DMA

Reactions

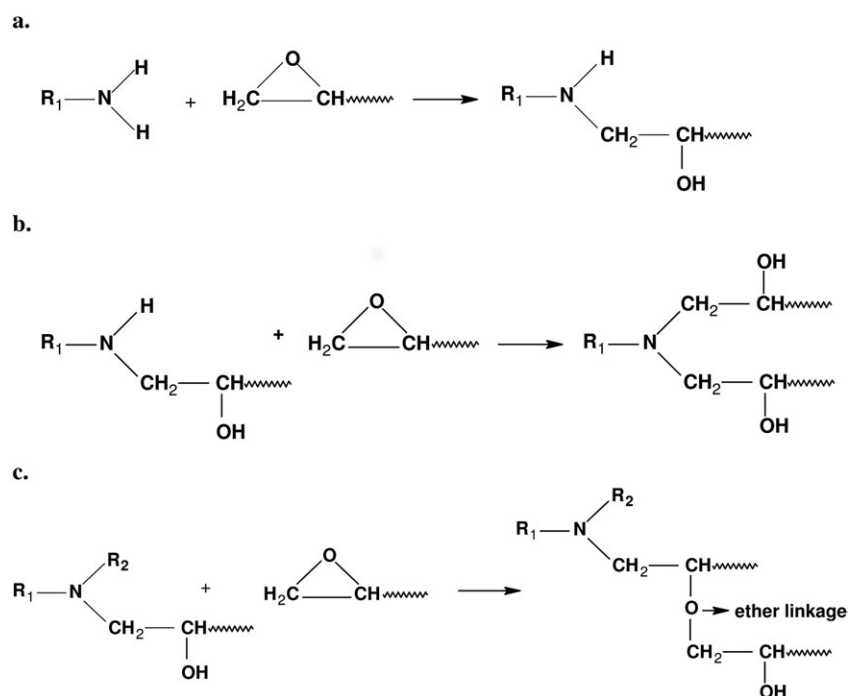


Figure 1. (a) Epoxide ring-opening reaction with primary amine b. Epoxide ring-opening reaction with secondary amine, c. Etherification reaction between hydroxyl group of reacted epoxy and unreacted epoxy groups (usually occurs at temperatures above 100°C) (or) homo polymerization of epoxy.

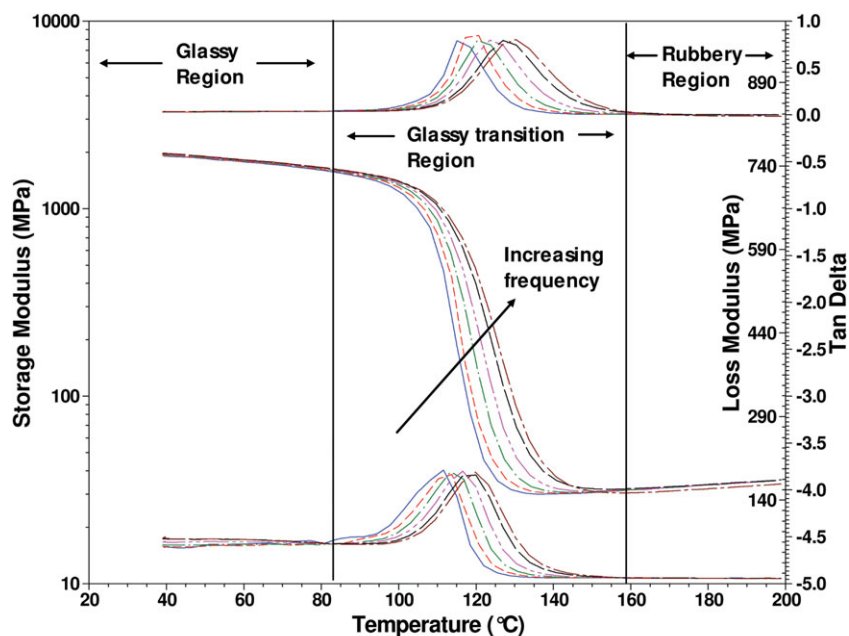


Figure 2. Damping ($\tan \delta$)[top], storage modulus (E')[middle], loss modulus[bottom] and versus temperature. Each line corresponds to the modulus response with respect to temperature at different frequencies (0.32, 1, 3.2, 10, 32, and 60 Hz). [Color figure can be viewed in the online issue, which is available at wileyonlinelibrary.com.]

characterization. All the samples in the two model systems are cured such that 100% conversion of the epoxy (or ideal network) is obtained. The samples that have undergone 100% epoxy conversion did not show epoxy group or oxirane ring at $\sim 912\text{ cm}^{-1}$ in the Fourier transform infrared (FTIR) spectroscopic studies. The 100% of epoxy could not be attained at higher curing temperature for the sample E4 in the model system I and for samples P3 and P6 in model System II.

FTIR Studies

The FTIR studies are conducted in the midinfrared region in ATR (Attenuated Transmission Reflectance) mode for understanding the percentage conversion in the cured samples. Different kinds of peaks due to bond stretching, bending, rocking, scissoring, etc. can be obtained from the FTIR spectra in the Mid-IR region.¹⁶ The reacting epoxy-amine mixture and their reacted product can be followed with different peaks, but only the peaks of interest such as the reacting peaks i.e., epoxy group or oxirane ring at $\sim 912\text{ cm}^{-1}$, amine N-H stretching at $\sim 3335\text{ cm}^{-1}$ and $\sim 719\text{ cm}^{-1}$, reference peaks (i.e., aromatic ring at $\sim 1607\text{ cm}^{-1}$, aliphatic C-H at $\sim 2855\text{ cm}^{-1}$), peaks of reacted product (e.g., hydroxyl group at 3500 cm^{-1}) are considered for following the epoxy-amine reaction. The % conversion of the epoxy is determined using eq. (1).

$$\text{Conversion } (p) = 1 - \frac{R_g(0)}{R_g(t)} \quad (1)$$

Where,

$R_g(0)$ = The ratio of peak area of a reacting group to reference peak area at time ($t = 0$),

$R_g(t)$ = The ratio of peak area of a reacting group to reference peak area at time (t),

Viscoelastic Measurement

A TA-Instruments Q800 model (Dynamic Mechanical Analyzer) was used. The viscoelastic study of cured resins was done on rectangular bars of specimen's in tension mode at different frequency sweeps (0.3–60 Hz) with a heating rate 1°C min^{-1} . Evolution of storage modulus (E') and energy dissipation ($\tan \delta$) with temperature was measured (Figure 2).

Density

The densities of the cured resins are measured using the Archimedes principle that states that the volume is proportional to the difference in weight between a dry and submerged sample. The experimental set up consists of weighing balance and glass filled with silicone oil (Type: M100, Dow Corning). The sample weight is determined both in air and oil. The density is calculated using eq. (2).

$$\text{Density } (\rho) = \frac{\rho_{\text{oil}} \times \text{Sample}_{\text{dry}}}{\text{Sample}_{\text{dry}} - \text{Sample}_{\text{wet}}} \quad (2)$$

ρ_{oil} is the density of silicone oil (0.965 g/cm^3), $\text{Sample}_{\text{dry}}$ is the weight in grams of the sample in air and $\text{Sample}_{\text{wet}}$ is the weight in grams of the sample in silicone oil. The test procedure was calibrated with polystyrene and polycarbonate samples of known density.

CALCULATION OF INITIAL, NETWORK AND PHYSICAL PROPERTIES

Initial Properties-Average Functionality and Stoichiometric Ratio

Let us consider an arbitrary mixture of polydisperse monomers A_i with f_i functional groups and monomers B_j with g_j

functional groups. The number average functionalities then become

$$\bar{f}_{n,A} = \frac{\sum n_{Ai0}f_i}{\sum n_{Ai0}}, \quad \bar{g}_{n,B} = \frac{\sum n_{Bj0}g_j}{\sum n_{Bj0}} \quad (3)$$

in which n_{Ai0} and n_{Bj0} denote the initial number of moles of A_i and B_j monomers, respectively. For future use we also define the mole fractions of crosslinkable A and B groups a_i and b_j as

$$a_i = \frac{n_{Ai0}f_i}{\sum n_{Ai0}f_i}, \quad b_j = \frac{n_{Bj0}g_j}{\sum n_{Bj0}g_j} \quad (4)$$

and the stoichiometric ratio as the initial ratio of all available A groups to those of all B groups

$$r_A = \frac{\text{initial no. A groups}}{\text{initial no. B groups}} = \frac{\sum n_{Ai0}f_i}{\sum n_{Bj0}g_j} \quad (5)$$

For equal numbers of A and B groups this ratio equals unity. Consider now the case that there are more B groups available ($r_A < 1$) and that the A groups have reacted to extent p_A (defined as the number of reacted A groups divided by the initial number of A groups). Since the number of reacted B groups equals that of the reacted A groups the conversion of B, denoted as p_B , can then be expressed as

$$p_B = \frac{\text{no. reacted B groups}}{\text{initial no. B groups}} = \frac{\text{no. reacted A groups}}{\text{initial no. B groups}} = p_A r_A \quad (6)$$

Network Properties-Crosslink Density

To relate the resin chemistry to viscoelastic behavior the crosslink density has to be determined. The calculated crosslink density ($v_c^{M\&M}$), which is a function of conversion (p_A), mixing ratio (r_A), and functionality (f_i) can be determined from the Miller and Macosko theory,¹⁷ and is given by the relation

$$v_c^{M\&M} = \frac{\sum_{m=3}^{f_k} \frac{m-2}{2} \sum_{f_i=m}^{f_k} n_{Ai0} P_{m,f_i}(x)}{V} \quad (7)$$

Where n_{Ai0} is the molar concentration of A_f , V is the network volume related to mass network (M_n) and density (ρ) of the fully cured epoxy material as shown in eq. (8)⁸

$$V = \frac{M_n}{\rho} \quad (8)$$

and $P_{m, f_i}(x)$ and the probability that an A_f monomer has become an effective crosslink of degree m given by relations

$$P_{m,f_i}(x) = \binom{f_i}{m} x^{f_i-m} (1-x)^m \quad (9)$$

and x stands for the probability that a randomly picked A_f group is connected to a finite chain (dangling end). This quantity follows by solving

$$p_A \sum b_{gj} \left[1 - r_A p_A (1 - \sum a_i x^{f_i-1}) \right]^{g_j-1} - x - p_A + 1 = 0 \quad (10)$$

Where $0 < x < 1$. A numerical solution for x is readily obtained with mathematical tools like MatLab. For the system $A_2 + A_3 + A_4 + B_2$, however, a closed form solution exists:

$$x = \frac{\sqrt{a_3^2 - a_4(3a_4 + 2a_3 + 4a_2 - \frac{4}{r_{APA}})} - a_3}{2a_4} - \frac{1}{2} \quad (11)$$

An example to calculate the crosslink density using Miller Macosko's theory formula for the sample that is formed by reacting 2 moles of BADGE (Bisphenol A diglycidyl ether) and 1 mole of EDA (Ethylene diamine) to form ideal network. The functionality of BADGE is 2 i.e., $f_E = 2$ and the functionality of EDA is 4 i.e., $f_A = 4$ and the stoichiometric balance ($r = 1$). For the above system, eq. (10) reduces to

$$x^3 - (1/p^2)x - 1 + 1/p^2 = 0 \quad (12)$$

In the case of ideal network formation $p = 1$. The value of x is 0 at $p = 1$ since there are no finite chains at complete conversion. From eq. (9), the probability that the reactants EDA have reacted is $P_{3,4}(x) = 0$ and $P_{4,4}(x) = 1$. Since, BADGE and EDA molecules that have reacted only once or twice do not contribute to the crosslink density, the total moles of chain ends bound at junction points is: $3P_{3,4}(x) + 4P_{4,4}(x) = 3(0) + 4(1) = 4$ moles. Since there are 4 moles of bound chain ends, the number of moles of elastically effective chains is $4/2 = 2$, and the crosslink density ($v_c^{M\&M}$) = $2/(\text{volume at conversion } (p) = 1) = 2/612.24 = 3.22 \times 10^{-3} \text{ mol/cm}^3 = 3266 \text{ mol/m}^3$.

Physical Properties-Glass Transition Temperature (T_g)

One way of defining the glass transition temperature is by determining the temperature at the peak maximum of the $\tan \delta$ curve for 1 Hz and is denoted by $T_g^{\tan \delta}$ in this article. Further, the glass transition temperature can also be predicted using DiMarzio equation and is denoted by T_g^{DiM} and is defined by eq. (13).

$$T_g^{DiM} = \frac{T_{gl}}{(1 - K_{DM} F v_c^{M\&M})} \quad (13)$$

Where T_{gl} is the T_g of the uncrosslinked or linear polymer chain, K_{DM} is constant, F is the flexibility parameter in g/mole and $v_c^{M\&M}$ is the calculated crosslink density in mole/g. The T_{gl} can be predicted according to Van Krevelen and Hoftyzer's approach. Van Krevelen and Hoftyzer used the principle of molar additivity to determine the T_g for linear polymers.¹⁸ The T_{gl} is predicted using the eq. (14).

$$T_{gl} = \frac{Y_g}{M} = \frac{\sum_i Y_{gi}}{M} \quad (14)$$

Where Y_g is the molar glass transition function (kg/mol), T_g is the glass transition temperature and M is the molecular weight of the repeating unit and $\sum Y_{gi}$ is the sum of the individual group contributions. The values of Y_g are taken from Van Krevelen's book.¹⁸ Further, the eq. (13) can be written as

$$T_g^{DiM} = T_{gl} \left(1 + \frac{K_{DM} F v_c^{M\&M}}{1 - K_{DM} F v_c^{M\&M}} \right) \quad (15)$$

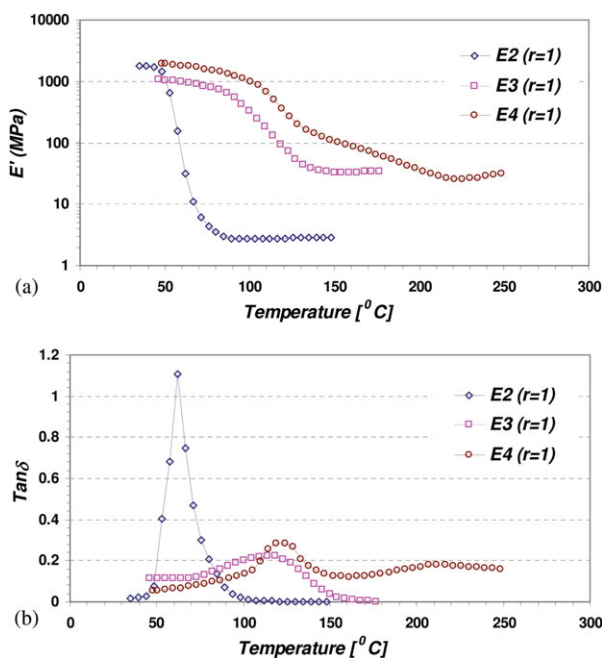


Figure 3. (a) Storage Modulus (E') versus temperature at 1 Hz frequency of Model I samples. (b) $\text{Tan } \delta$ response versus temperature at 1 Hz frequency for Model I samples. [Color figure can be viewed in the online issue, which is available at wileyonlinelibrary.com.]

The eq. (15) is similar to Fox-Losheak equation¹⁹ as shown by eq. (16).

$$T_g = T_g^{\infty} \left(1 + K_{FL} \left[\frac{v_c^{M\&M}}{1 - v_c^{M\&M}} \right] \right) \quad (16)$$

Where K_{FL} is constant.

RESULTS AND DISCUSSION

DMA Studies

The Figure 2 shows the experimental data of the storage modulus data versus the temperature at different frequencies (0.32, 1, 3.2, 32, and 60 Hz) for the epoxy sample A4.¹⁰ The sample A4 is formed by reaction of Bisphenol A diglycidyl ether (BADGE) and ethylene diamine. The experimental storage modulus contains three regions i.e., glassy plateau, rubbery plateau, and transition region. The modulus in the glassy plateau is termed as glassy modulus and denoted by E_g . Rubbery modulus (E_r) is defined as the modulus in the rubbery region. The glass transition temperature T_g from DMA experiments can be determined from the storage modulus, loss modulus and $\text{tan } \delta$ curves. The glass transition temperature T_g in this article is determined using the $\text{tan } \delta$ curve and is denoted by $T_g^{\text{tan } \delta}$. The $T_g^{\text{tan } \delta}$ is the temperature at the peak maximum of the $\text{tan } \delta$ curve for 1 Hz. The values of E_g and E_r are the storage modulus at $T_g - 60^{\circ}\text{C}$ and $T_g + 30^{\circ}\text{C}$.

Analysis of E_g , E_r and $T_g^{\text{tan } \delta}$

In model System I, the functionality of the initial epoxy reactant is varied from $f_E = 2$ to $f_E = 4$ and the functionality of the amine is 2 i.e., $f_A = 2$ [see Table I]. The viscoelasticity for the

samples $E2 (r = 1)$, $E3 (r = 1)$, and $E4 (r = 1)$ are shown in Figure 3(a). From Figure 3(a) it can be seen that the 1 Hz data for the sample $E4 (r = 1)$ in its rubbery region does not have a clear rubbery plateau. This can be because of incomplete reaction between the epoxy and amine. Moreover the $\text{tan } \delta$ peak for the sample $E4 (r = 1)$ showed two $\text{tan } \delta$ peaks at 122 and 207 $^{\circ}\text{C}$ which occurs during the temperature scan [Figure 3(b)]. The appearance of two $\text{tan } \delta$ peaks indicate heterogeneous network. The second $\text{tan } \delta$ peak at 207 $^{\circ}\text{C}$ could be because of the reaction of the remaining epoxy groups. To assure that the sample $E4$ is fully cured the sample $E4$ is further cured at 250 $^{\circ}\text{C}$ for 30 min. Figure 4 shows the viscoelastic data for 1 Hz frequency for the sample $E4 (r = 1)$ cured at 250 $^{\circ}\text{C}$ for 30 min. It can be seen that a single $\text{tan } \delta$ peak is observed. This indicates homogeneity and also the modulus in the rubbery region decreased with the increase in temperature. Also around 300 $^{\circ}\text{C}$ there is a sudden drop in the rubbery modulus which is an indication of degradation.²⁰ The temperature at the $\text{tan } \delta$ peak maximum for 1 Hz frequency which is the glass transition temperature is found to be 109 $^{\circ}\text{C}$. This is lower than the T_g (118 $^{\circ}\text{C}$) of sample $E3 (r = 1)$. This means that the degradation leading to the decrease in the T_g as well as the reaction of the remaining epoxy units takes place at the same time. This is mainly due to the steric hindrance caused by the rigid aromatic structure within the TPGE epoxy resin in the $E4 (r = 1)$ sample. Since 100% conversion of epoxy groups for the sample $E4 (r = 1)$ is not possible and also the T_g determined for the sample $E4$ cured at 250 $^{\circ}\text{C}$ for 3 h does not contain an ideal network. So, the T_g data of $E4 (r = 1)$ cannot be taken for the analysis as it would lead to erroneous interpretation of the T_g results. Hence the viscoelastic data for the sample $E4 (r = 1)$ is omitted for the analysis. The analysis of the viscoelastic data for the samples $E2 (r = 1)$ and $E3 (r = 1)$ is discussed below.

The increase in the functionality of the initial epoxy reactant showed that the E_g values of the cured epoxy remained constant (~ 1800 MPa) (see Table IV). While, E_r increased from 3 to 28 MPa. The crosslink density can be determined from E_r using eq. (17). The crosslink density that is determined from E_r is the measured crosslink density (v_c^{meas}).

$$E_r = 3A v_c^{\text{meas}} RT \quad (17)$$

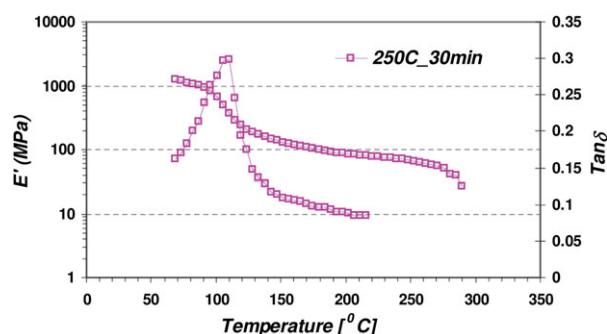


Figure 4. Storage Modulus (E') and $\text{tan } \delta$ versus temperature at 1 Hz frequency of the $E4$ sample cured at 250 $^{\circ}\text{C}$ for 3 h. [Color figure can be viewed in the online issue, which is available at wileyonlinelibrary.com.]

Table III. The Samples of the Two Model Systems with Their Mixing Ratio (r), Conversion (p), Measured and Predicted Crosslink Densities, Flexibility Parameter (F), T_g of Linear Polymer (T_g^1), measured and Predicted T_g

Model no.	Sample code	r	p	Crosslink density (v_c) [mol/m ³]		F [g/mol]	T_g^1	T_g [°C]		PWHH [°C]
				Measured v_c^{meas} eq. (17)	Predicted $v_c^{M\&M}$ eq. (7)			Measured	Predicted T_g^{DiM} eq. (13)	
I	E2	0.95	1	0	0	22.75	65 [#]	64	65	-
	E2.5	0.95	1	1163	1024	21.54	73 [#]	90	93	29
	E3	0.95	1	2262	2030	20.33	82 [#]	117	121	35
II	P1	1	1	1861	2039	22.83	72 [#]	121	116	15
	P3	1	0.99	1561	1767 ^{ft}	26.57	59 [#]	98	103	15.2
	P6	1	0.96	1010	1095 ^{ft}	32.17	45 [#]	82	80	12

Mod. No, Model Number; Sam Cod., sample code; T_g^{DiM} , T_g determined using DiMarzio approach; T_g^{DiB} , T_g determined using DiBenedetto's approach; ft, Calculations based on % conversion determined using FTIR; v_c^{meas} Crosslink density calculated from rubbery modulus using theory of rubber elasticity; $v_c^{M\&M}$, crosslink density calculated using Miller and Macosko's Theory; #, calculated by fitting the values of $T_g^{V\&H}$, K_{DM} , F values to DiMarzio's equation.

The values of the v_c^{meas} for the two model systems are shown in Table III. The crosslink density can be also calculated from Miller and Macosko theory. The calculated crosslink density i.e., $v_c^{M\&M}$ values for all the samples in model systems (see Table III) can be compared with that of Halary.²¹

Also, the $T_g^{\text{tan}\delta}$ increased from 64 to 117°C [see Table III]. The constant value of E_g in Table IV around 1800 MPa can be due to the restricted molecular motion below T_g . The increase in the E_r and $T_g^{\text{tan}\delta}$ is due the increase in the $v_c^{M\&M}$ [see Table III].

The sample $E2(r = 1)$ is formed by due to the reaction between BFDGE ($f_E = 2$) and DMEDA ($f_A = 2$) it is expected to contain uncrosslinked linear chains within the sample and hence should be thermoplastic in nature (see Table II). It means that with the rise in temperature, the characteristic property of thermoplastics to melt or flow at a certain temperature should lead to a drop in the modulus, which approaches zero at higher temperatures. It can be observed from Figure 3(a) that the sample $E2$ ($r = 1$) clearly shows a rubbery plateau which indicates that the sample contains a small fraction of partly crosslinked network chains. This could be because of the reaction of hydroxyl groups (obtained from the reaction of epoxy-amine) with the remaining epoxy groups (Figure 1(c)). This is also called homopolymerization. So, in order to avoid the crosslinked network state within the sample $E2$ ($r = 1$) a new mixture is made by mixing 0.5 wt % excess amine to the BFDGE-DMEDA stoichiometric mixture. Similarly, 0.5 wt % excess amine is added to the stoi-

chiometric mixture of TMTE-DMEDA. Both mixtures are then cured according to the cure schedules specified in Table II and are characterized in DMA. Figure 5 shows the E' and $\tan \delta$ data for 1 Hz frequency for both formulations. The sample $E2$ containing excess of amine did not show a rubbery plateau and also the sample melted in the DMA during characterization as expected. The DMA data of $E2$, $E2.5$ (mixture of $E2$ and $E3$) and $E3$ containing 0.5% wt % excess of amine is shown in Tables III and IV. The samples $E2$, $E2.5$ (mixture of $E2$ and $E3$) and $E3$ containing 0.5% wt % excess of amine have mixing ratio ($r = 0.95$). The samples $E2$, $E2.5$ and $E3$ and $E2$ ($r = 1$), $E3(r = 1)$, and $E4$ ($r = 1$) have similar cure and post cure schedules.

In model System II, the functionality of the epoxy and amine is constant i.e., $f_E = 2$ and $f_A = 3$. While, the side (or pendant) chain length of the amine reactant is varied as shown in Table I. The increase in the pendant chain length showed that the E_g values of the cured epoxy remained constant (~ 1800 MPa) (see Table IV). While, E_r decreased from 20 to 8.5 MPa. Also, the $T_g^{\text{tan}\delta}$ decreased from 121 to 82°C (decreased by 39°C). The Table IV shows that the glassy modulus (modulus at $T_g - 60^\circ\text{C}$) remains constant, i.e. independent of the increase in pendant chain length. It means that the introduction of pendant chains within the network structure does not have any affect on the glassy modulus. The restriction of molecular motion below T_g to transitions over a few atoms length (which is much smaller

Table IV. The Parameters E_r , E_g , τ_0 , τ_g , and χ Fitted to the KWW Equation to Generate Experimental Master Curves

Model no.	Sample code	E_r	E_g	τ_0 [s]	τ_g [s]	χ
I	E2	0	1898	2.63E-06	1.98	0.20
	E2.5	12	1891	0.0142	0.68	0.149
	E3	25	1970	6.45E+03	0.81	0.197
II	P1	20	1875	6.09E+05	0.122	0.232
	P3	16	2176	5.39E-02	0.142	0.328
	P6	8.5	2070	5.78E-05	0.062	0.246

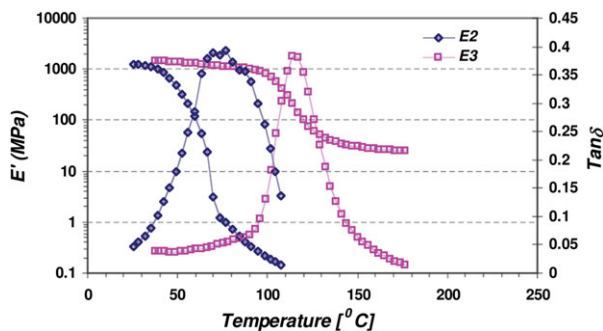


Figure 5. Storage Modulus (E') and $\tan \delta$ versus temperature at 1 Hz frequency of Model I samples. [Color figure can be viewed in the online issue, which is available at wileyonlinelibrary.com.]

than the size of a pendant chain) is the reason for the independency of the glass modulus for the samples $P1$, $P3$, and $P6$.

The decrease in the rubbery modulus decreases with the increase in the pendant chain length is not expected. The functionality of the epoxy and amine reactants are constant and therefore the cured epoxy materials are expected to have identical crosslink density values. The FTIR results of DER 332 and the sample $P1$ is shown in Figure 6. The absence of oxirane peak at $\sim 912\text{ cm}^{-1}$ indicates that 100% epoxy conversion is attained. The FTIR results of sample $P3$ cured at 200°C for 2 h and sample $P6$ cured at 100°C for 2 h, 200°C for 4 h, 250°C for 3 h is shown in Figures 7 and 8. The FTIR results of the samples $P3$ cured at 200°C for 2 h and $P6$ cured at 200°C for 4 h showed 99% and 96% of epoxy conversion. Consequently,

there are still epoxy groups remaining in the network of the cured samples. These will remain in the network structure as dangling ends (or) pendant groups. The incomplete reaction of epoxy in the $P3$ and $P6$ samples should decrease the number of crosslinking sites from the ideal network formation. This incomplete conversion was taken into account while calculating the crosslink density using the M&M theory in eq. (7). Also, the increase in the chain length of the pendant chain introduces flexibility in the network. The effect of the flexibility on the T_g was studied by DiMarzio and Bellenger.^{22,23} According to DiMarzio's approach, the T_g can be predicted using the eq. (13). In eq. (13), the flexibility (F) is calculated using eq. (18).

$$F = \frac{\sum N_i F_i}{\sum N_i} \quad (18)$$

Where N_i is the number of crosslink reactants of type i (whose flex param F_i) in the repeating unit of the network.

Finally, the T_g of all the samples in the two model systems are predicted using the DiMarzio's approach [eq. (13)] and is shown in Figure 9. The Figure 9 shows the plot of predicted T_g (T_g^{DiM}) versus measured T_g ($T_g^{\tan\delta}$). It can be seen that $T_g^{\tan\delta}$ is predicted quite well. In conclusion, the T_g is mainly dependent on two parameters i.e., crosslink density and flexibility.

PWHH

For a systematic analysis of the broadness of the $\tan \delta$ curve for all the samples in the two model systems, the width of the $\tan \delta$ curve at half height for 1 Hz is taken and is denoted as PWHH [Peak width at half height]. To determine the peak

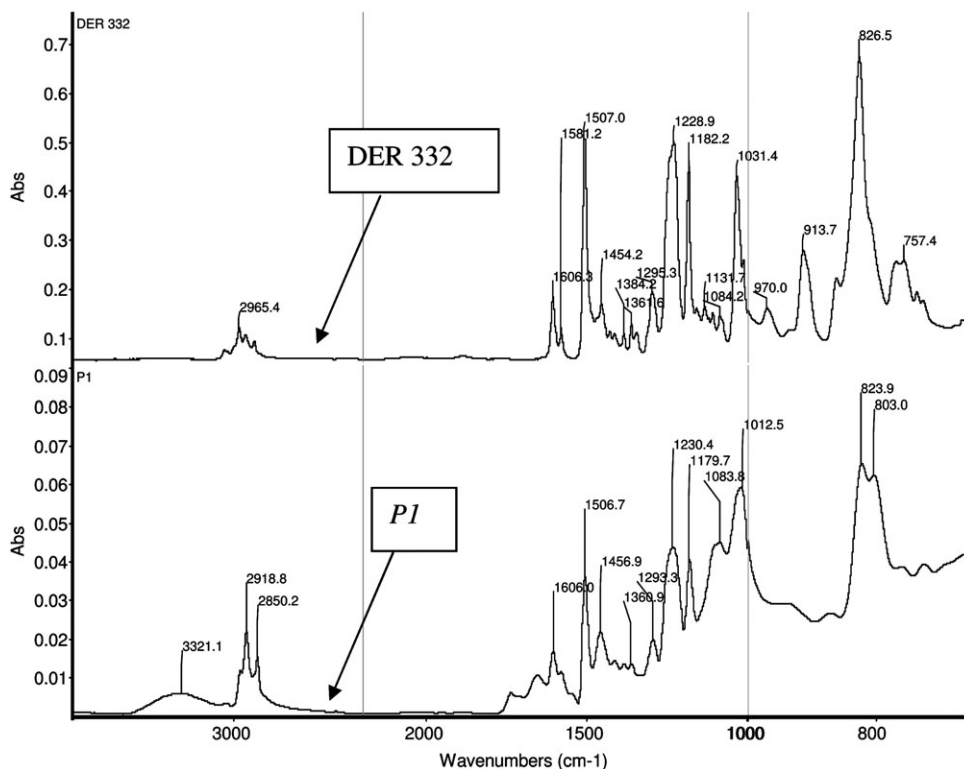


Figure 6. Mid-infrared spectrum for pure BADGE (DER 332) epoxy and sample $P1$ cured at 150°C for 4 h.

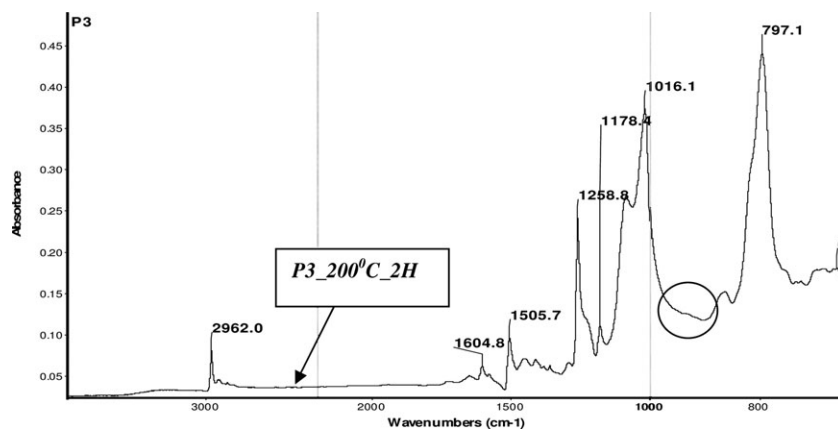


Figure 7. Mid-infrared spectrum of the sample P3 cured at 200°C for 2 h.

width at half height (PWHH) for the $\tan \delta$ curve a baseline is drawn connecting the initial rise and final drop of the $\tan \delta$ curve and then a line is drawn from the centre of the baseline towards the $\tan \delta$ peak as shown in the Figure 10. The width at half height of the $\tan \delta$ peak is the PWHH. PWHH indicates the temperature increase which is needed for the crosslinked network to undergo the relaxation process i.e., from glassy state to rubbery state.

The PWHH for all the samples in the two model systems are shown in Table III. Table III shows that the PWHH increases from E2 to E3 in the model System I. This is mainly because of the fact that with the increase in the epoxy functionality in the reacting mixture, the increase in the crosslink density of the cured network occurs. On molecular scale, as the crosslink

density increases the number of crosslinking points increases and therefore the network structure comes closer and thus shows a higher $T_g^{\tan \delta}$. After reaching $T_g^{\tan \delta}$ the free volume plays an important role on the molecular mobility. Since the cross-linked network containing a higher crosslink density will generate less free volume and so it takes more temperature to undergo the relaxation process i.e., to reach from the glassy state to rubbery state. So, in the Model I system the sample E3 has the highest crosslink density and therefore it shows the maximum PWHH. From Figure 5, the damping data for E2 above 110°C does not exist as the sample has melted during the DMA run. This confirms that the sample E2 is thermoplastic in nature. Since the $\tan \delta$ data above 110°C of E2 is absent a baseline cannot be drawn for the determination of the height as

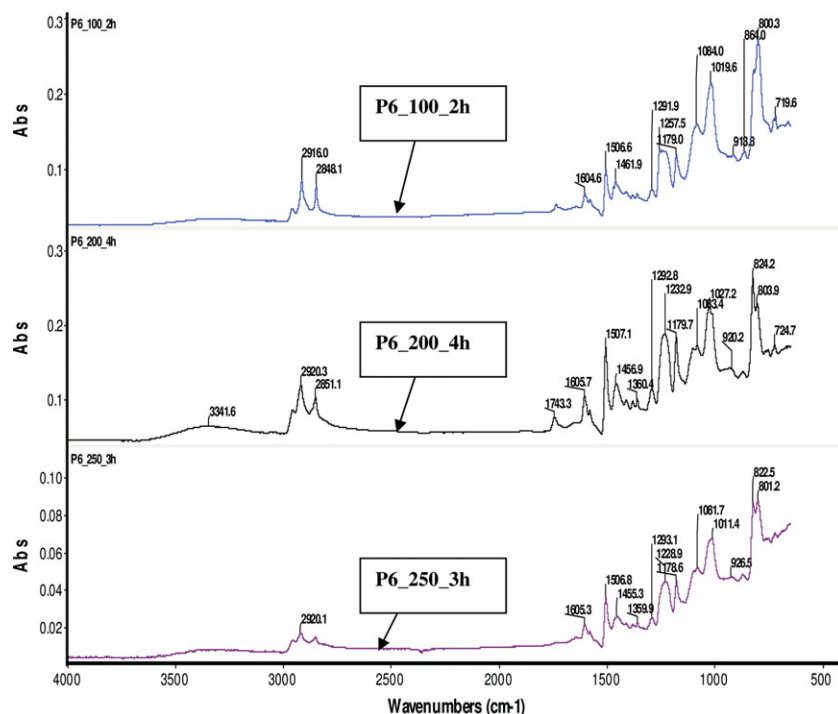


Figure 8. Mid-infrared spectrums for sample P6 cured at i. 100°C for 2 h ii. 200°C for 4 h iii. 250°C for 3 h. [Color figure can be viewed in the online issue, which is available at wileyonlinelibrary.com.]

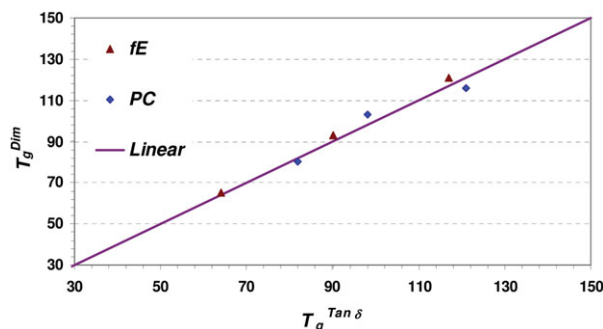


Figure 9. Predicted T_g (T_g^{Dm}) versus measured T_g ($T_g^{\tan \delta}$). [Color figure can be viewed in the online issue, which is available at wileyonlinelibrary.com.]

well the width of the $\tan \delta$ curve. To obtain at least an estimate we take that $\tan \delta = 0$ line as the baseline and determine the PWHH to be about 55°C . The extremely wide peak for the linear system suggests a broad distribution in the length of the linear chains. The smallest chains start to move already at room temperature whereas the longest ones only commence at above 100°C . Since the $\tan \delta$ peak height and the width of the sample $E2$ cannot be determined, the PWHH data of $E2$ cannot be compared with $E2.5$ and $E3$. However, it can be observed from Table III that the $T_g^{\tan \delta}$ and the PWHH increase from $E2.5$ and $E3$. This trend is expected since the crosslink density of $E3$ is higher in comparison to $E2.5$. Figure 11 a & b, shows the storage modulus and damping curve for the model system II.

In model System II, the PWHH values are expected to increase from $P1$ to $P6$. From table it can be seen that the PWHH increased from $P1$ to $P3$ as expected, whereas the PWHH for the sample $P6$ decreased. The unexpected decrease in the PWHH for the sample $P6$ in Figure 12 is mainly due to the lower % of conversion of epoxy groups (i.e., 95% conversion).

Finally, the PWHH of all the samples in the two model systems are plotted against crosslink density ($v_c^{M\&M}$). It is found that the PWHH does not scale with respect to $v_c^{M\&M}$. When the PWHH is plotted against the flexibility (F). It can be seen from Figure 12 that the PWHH decreases linearly with the increase in the flexibility. The decreasing trend of PWHH in Figure 12

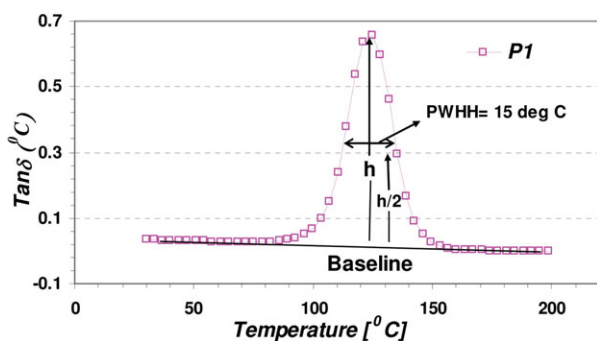


Figure 10. Plot of $\tan \delta$ versus temperature for sample $P1$. The peak height is indicated by h and the width at half height of $\tan \delta$ curve is indicated by PWHH. [Color figure can be viewed in the online issue, which is available at wileyonlinelibrary.com.]

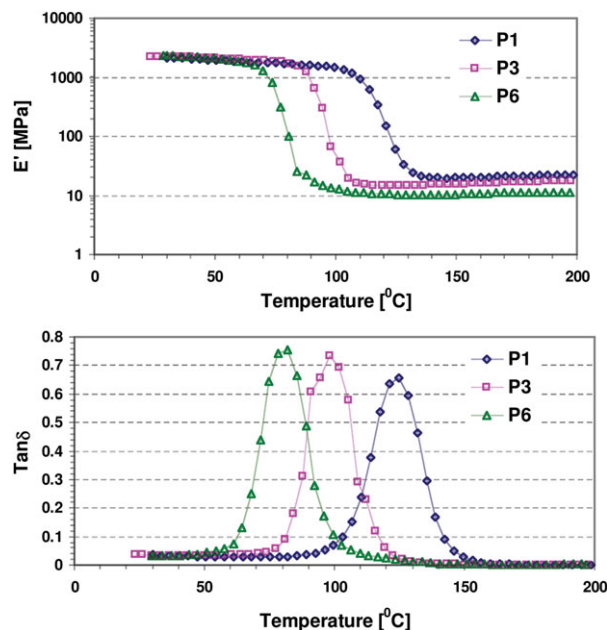


Figure 11. (a) Storage Modulus (E') versus temperature at 1 Hz frequency of Model II samples. (b) $\tan \delta$ response versus temperature at 1 Hz frequency for Model II samples. [Color figure can be viewed in the online issue, which is available at wileyonlinelibrary.com.]

shows that the co-operativity or extent of motions in the transition region is dependent on the flexibility (F). As the flexibility (F) indicates the concentration of the flexible bonds (aliphatic) in the network, it can be concluded that the increase in the concentration of the aliphatic chain length in the network causes the decrease in the PWHH. On the other hand the increase in the aromatic content in the network should increase the PWHH. The expected trend as discussed above is clearly observed in the Model I system (see Table III). The sample $E3$ which has the highest number of aromatic groups showed the least flexibility (F) and the highest PWHH out of the two model systems. Also, the PWHH shows a better scaling with respect to the flexibility as shown in Figure 12.

Modeling of the Viscoelastic Master Curves

The properties of the epoxy thermosets vary with temperature as well as time. The incorporation of time (or frequency) dependency on the viscoelasticity is very important. This can be

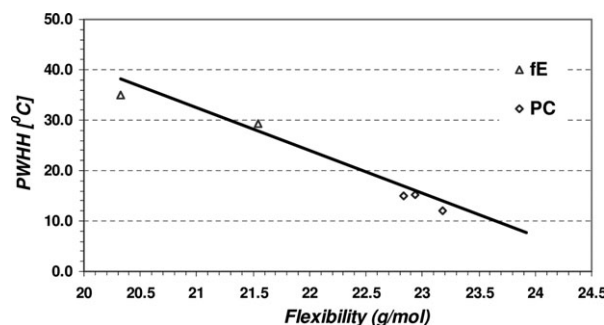


Figure 12. The peak width at half height of the $\tan \delta$ curve of all model systems with respect to flexibility (F).

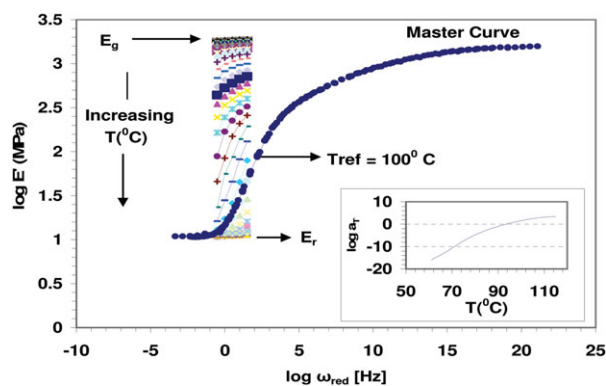


Figure 13. Storage modulus (E') response with respect to the reduced frequency (ω_{red}) for a typical cured epoxy sample characterized in the DMA. E_g , E_r , and T_{ref} are the glassy modulus, rubbery modulus and the reference temperature. The symbol led lines (.) are the modulus values of all frequencies at different temperatures. The master curve is shown by a full line (—). A plot of the shift factor ($\log a_T$) versus temperature is shown as an insert. [Color figure can be viewed in the online issue, which is available at wileyonlinelibrary.com.]

done by constructing a viscoelastic master curve using the Time Temperature Superposition principle. The storage modulus data at different temperatures is plotted with respect to frequency scale for the epoxy sample A4¹⁰ that is characterized in the DMA experiment (Figure 13). According to Time Temperature Superposition principle^{24,25} the modulus data can be shifted along the time (or frequency) axis to generate a so-called master curve (included in Figure 13). Figure 13 shows the procedure for the generation of the storage modulus master curve plotted against reduced angular frequency (ω_{red}) obtained after shifting the modulus data on frequency to a reference temperature ($T_{\text{ref}} = 100^\circ\text{C}$).^{26,27} Where ω_{red} is given by

$$\omega_{\text{red}} = \frac{\omega}{a_T} \quad (19)$$

And ω is the angular frequency (rad/s) and a_T is the shift factor. The corresponding shift factor is shown as an insert in Figure 13. From Figure 13 it can be seen that the glassy modulus (E_g) is observed at higher frequency and the rubbery modulus is seen at lower frequency on the Master Curve. Similarly, E'' (Loss modulus) and $\tan \delta$ (Damping) master curves can also be obtained using the same shift factors. The storage modulus data generated a unique master curve using the shift factors. Initially, the storage modulus master curves were modeled using Hivri-liak Negami (HN) fit function.^{11,28} Also, mathematical model such as generalized Maxwell model can also be used to describe the storage modulus master curves.²⁹ Previously, research was done in modeling the viscoelastic curve using above models.^{1–6} The above models have two or more fit parameters that can describe the viscoelastic master curve quite accurately. On the otherhand, relating the viscoelastic master curve to the crosslink density ($v_c^{M\&M}$) via two fit parameters is difficult. In this paper, Kohlrausch-Williams-Watts (KWW) model containing single fit parameter χ is used. The KWW fit function gives the advantage of understanding the effect of $v_c^{M\&M}$ on the viscoelastic master curve via the parameter χ . In order to be able to predict the

viscoelastic master curve, firstly main features of all the master curves are fitted to the KWW-fit function [eq. (20)] to capture the viscoelastic parameters i.e., E_g , E_r , and χ

$$E' = E_r + (E_g - E_r) \exp[-(\omega_{\text{red}} \tau_0)^{-\chi}] \quad (20)$$

To compare the different experimental master curves it is necessary to use a common shift factor curve. A reference temperature (T_{ref}) is chosen to be T_0 and then the WLF (Williams-Landel-Ferry) fit parameters are determined.

$$\log a_T = \frac{-C_1^0(T - T_0)}{C_2^0 + (T - T_0)} \quad (21)$$

The common shift factor parameters that are determined are C_1^0 , C_2^0 . It is well known that the relaxation time constant (τ_0) in eq. (20) depends strongly on the temperature.

The WLF fit function [eq. (21)] algorithm in Matlab is discussed below.

```
WLF = inline(' - C(1)*T-T_0./
C(2)+T-T_0) ', 'C', 'T-T_0'); %WLF fit function [eq. (21)]
params 0 = [17 51] % The initial guess for
C_1^0 = 17 and C_2^0 = 51
params = nlinfit (T-T_0, log a_T,
WLF, params 0) % nonlinear curve fit to
determine C_1^0 and C_2^0
WLFfit = WLF (params, T-T_0) % WLF fit using the params
```

For thermorheological simple materials this temperature dependency can be taken into account with the so called shift function $a_T(T, T_{\text{ref}}) = \tau_0(T)/\tau_0(T_{\text{ref}})$. Where, τ_0 is determined by taking the reference temperature in eq. (22).

$$\tau_0 = \tau_{0g} a_T(T_0, T_g^{DiM}) \quad (22)$$

Here T_g^{DiM} is dependent on the crosslink density as well as the flexibility of the network. Now, the determined common shift factors C_1^0 , C_2^0 are used for obtaining new master curves and can be called Local fit master Curves. Fitting the KWW-function to local fit master curves generated different values of χ , E_g , and E_r within each system. In order to be able to describe the relaxation curve of all the master curves within each model system a global model which contains fixed values for the parameters χ and E_g has to be predicted. Note: The values of E_r and τ_0 are dependent on the crosslink density of the network and therefore can change. Finally, the predicted global master curves are generated using parameters χ , E_g , E_r , and τ_0 and are subsequently compared with the experimental master curves. The fit parameters determined by following the above mentioned procedure are shown in Table IV. Using these parameters and common shift factor parameters $C_1^0 = 18.3$, $C_2^0 = 79.9$, the experimental master curves are generated. Further, global master curves are generated using $\tau_g = 4.30 \times 10^{-4}$ and, $E_g = 1700$ MPa, $\chi = 0.176$ and common shift factor (or WLF parameters) $C_1^0 = 18.3$, $C_2^0 = 79.9$. The global master curves are then compared with experimental master curves and are discussed below.

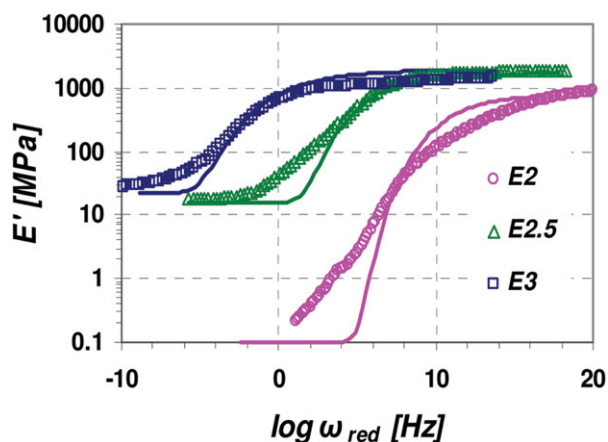


Figure 14. The experimental master curves (symbols) at $T_{ref} = 100^{\circ}\text{C}$ in comparison to the globally fitted master curves (full lines) for Model System I. [Color figure can be viewed in the online issue, which is available at wileyonlinelibrary.com.]

The Figures 14 and 15 show the experimental master curves (symbols) for the Model systems I and II. From Figure 14, it can be seen that with the increase in the epoxy functionality in the model System I the master curves shifted towards lower frequency scale. Note: the glass transition shifts from 10^{+9} to 10^{-3} with respect to reduced frequency. This means that there is a shift of 12 decades. As discussed earlier, the rubbery modulus (E_r) and T_g^{DiM} of the model system I increased with the amine and epoxy functionality. The shift in master curves, E_r and T_g^{DiM} in the Model System I is controlled by the crosslink density.

The master curves (Figure 15) of the Model System II shifted by 11 decades (from 10^{-7} to 10^{+4}) towards higher frequency scale with the increase in the pendant chain length i.e., from P1 to P6. Also the E_r decreased with the crosslink density. The T_g decreased with the increase in the pendant chain length from P1 to P6.

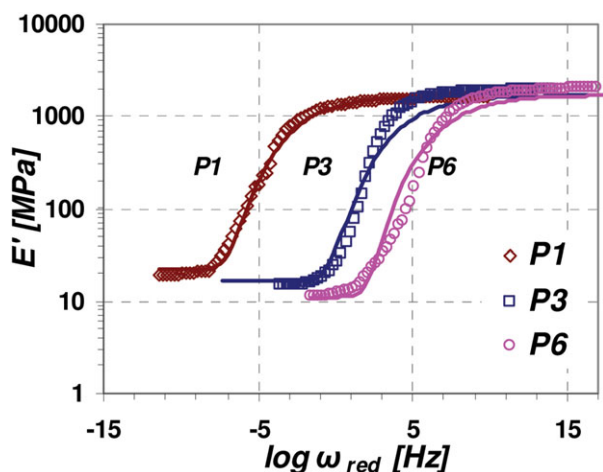


Figure 15. The experimental master curves (symbols) at $T_{ref} = 100^{\circ}\text{C}$ in comparison to the globally fitted master curves (full lines) for Model System II. [Color figure can be viewed in the online issue, which is available at wileyonlinelibrary.com.]

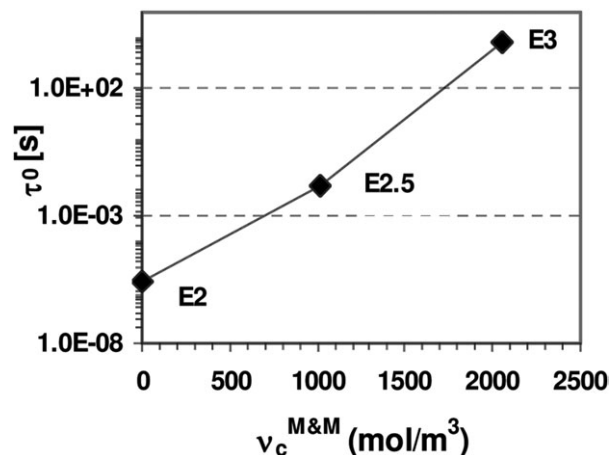


Figure 16. The relaxation time constant (τ_0) at $T_{ref} = 100^{\circ}\text{C}$ versus the predicted crosslink density (ν_c) for Model System I.

Moreover the relaxation time constant (τ_0) increased with the increase in the predicted crosslink density ($\nu_c^{M\&M}$) for the two model systems (Figures 16 and 17). The slope χ for Models I and II did not show any systematic trend with respect to the crosslink density ($\nu_c^{M\&M}$). From the above discussion it can be understood that by changing the parameters i.e., crosslink density and the flexibility, the relaxation of the viscoelastic master curves also change. The changes in the relaxation master curves are predicted quite well using global master curves (full lines) as shown in Figures 14 and 15 and so it can be concluded that the KWW fit function describes the relaxation master curves reasonably well.

CONCLUSIONS

In the model System I, the functionality of the initial epoxy reactant is increased in the epoxy-amine mixture. With the increasing epoxy functionality, the T_g and the E_r of the cured samples increased. The viscoelastic master curves which are generated using Time-Temperature-Superposition principle shifted

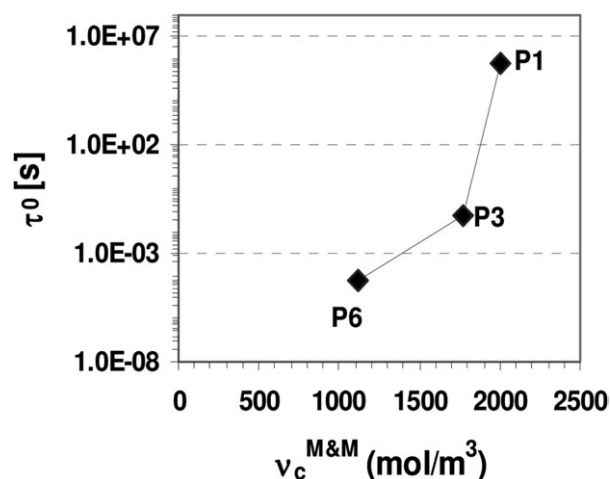


Figure 17. The relaxation time constant (τ_0) at $T_{ref} = 100^{\circ}\text{C}$ versus the predicted crosslink density (ν_c) for Model System II.

to lower frequency with the increasing epoxy functionality. While, the relaxation time constant (τ_0) increased. The increase in the T_g , E_p , and τ_0 is due to the increase in the crosslink density ($v_c^{M\&M}$). For the Model System II, the functionality of the initial epoxy and amine reactants are kept constant. While, the pendant chain length of the amine reactant is varied. With increase in the pendant chain length, the T_g and the E_r of the cured samples decreased. While, the viscoelastic master curves shifted to higher frequency. The relaxation time constant decreased with increasing pendant chain length. The decrease in the T_g , E_p , and τ_0 is due to the decrease in the crosslink density ($v_c^{M\&M}$) and the Flexibility (F).

REFERENCES

1. Simon, S. L.; Gillham, J. K. *J. Appl. Polym. Sci.* **1993**, *47*, 461.
2. Simon, S. L.; McKenna, G. B.; Sindt, O. *J. Appl. Polym. Sci.* **2000**, *76*, 495.
3. Li, Q. X.; Simon, S. L. *Macromolecules* **2007**, *40*, 2246.
4. Shimp, D. *J. Appl. Polym. Sci.* **1994**, *71*, 623.
5. Ho, T. H.; Wang, C. S. *Polymer* **1996**, *37*, 2733.
6. Lee, A.; McKenna, G. B. *Polymer* **1988**, *29*, 1812.
7. Banks, L.; Ellis, B. *Polymer* **1982**, *23*, 1466.
8. Vakil, U. M.; Martin, G. C. *J. Appl. Polym. Sci.* **1992**, *46*, 2089.
9. Gerard, J. F.; Galy, J.; Pascault, J. P.; Cukierman, S.; Halary, J. L. *Polym. Eng. Sci.* **1991**, *31*, 615.
10. Nakka, J. S.; Jansen, K. M. B.; Ernst, L. J.; Jager, W. F. *J. Appl. Polym. Sci.* **2008**, *108*, 1414.
11. Nakka, J. S.; Jansen, K. M. B.; Ernst, L. J. *J. Polym. Res.* **2011**, *18*, 1879.
12. Jansen, K. M. B. *Eng. Mater. Technol.* **2006**, *128*, 478.
13. Hill, L. H. *Prog. Organic Coat.* **1997**, *31*, 235.
14. Nielsen, L. E. *J. Macromol. Sci.-Rev. Macromol. Chem.* **1969**, *C3*, 69.
15. Nielsen, L. E. *Mechanical Properties of Polymers and Composites*, 2nd ed., Wiley, **1994**, p 141.
16. Stuart, B. *Infrared Spectroscopy: Fundamentals and Applications*; Wiley, **2004** p 46.
17. Miller, D. R.; Macosko, C. W. *Macromolecules* **1976**, *9*, 199, 206.
18. Van Krevelen, D. W.; Hoftyzer, P. J. *Properties of Polymers: Their Estimation and Correlation with Chemical Structure*, 2nd ed.; Elsevier: Amsterdam, **1976**.
19. Fox, T. G.; Flory, P. J. *J. Appl. Phys.* **1950**, *21*, 581.
20. Bicerano, J. *Prediction of Polymer Properties*, 3rd ed., New York: Dekker, **2002**, p 369.
21. Halary, J. L. *High Performance Polym.* **2000**, *12*, 141.
22. Bellenger, V.; Verdu, J. *J. Polym. Sci.: Part B: Polym. Phys.* **1987**, *25*, 1219.
23. Bellenger, V.; Dhaoui, W.; Verdu, J.; Galy, Won, Y. G.; Pascault, J. P. *Polymer* **1989**, *30*, 2013.
24. Ferry, J. D. *Viscoelastic Properties of Polymers*, 3rd ed.; **1976**, p. 271.
25. Ferry, J. D. *Viscoelastic Properties of Polymers*, Wiley: NY, **1980**.
26. Plazek, D. J.; Chay, C. *J. Polym. Sci. Part B: Polym. Phys.* **1991**, *29*, 17.
27. Plazek, D. J. *J. Rheol.* **1996**, *40*, 987.
28. Ivet Bahar, Burak Erman, George Fytas, Werner Steffen, *Macromolecules*, **1994**, *27*, 5200.
29. Daniel, J. O' Brien; Patrick, T. M.; Scott, R. W. *J. Compos. Mater.* **2001**, *35*, 883.